





# Anticancer and Multi-Biological Activities of Titanium Dioxide Nanoparticles Synthesized Using Lemon Peel Extract *via* Microwave Irradiation

Hayfa Habes Almutairi <sup>a</sup>, Nada H. Aljarba <sup>b</sup>, Abdulkarim S. Binshaya <sup>c</sup>, Adil Abalkhail <sup>d</sup> and Mohamed K. Y. Soliman <sup>e</sup>

Titanium dioxide nanoparticles (TiO<sub>2</sub> NPs) were synthesized using a microwave-assisted green synthesis approach using lemon peel extract as a reducing and stabilizing agent. The synthesized nanoparticles were characterized using UV–Vis spectroscopy, FTIR, TEM, SEM–EDX, and DLS analyses, which confirmed the formation of predominantly spherical nanoparticles with average particle sizes ranging from 25.6 to 38.7 nm. The biological activities of the synthesized TiO<sub>2</sub> nanoparticles were evaluated through different *in vitro* assays. The nanoparticles exhibited promising anticancer activity against HepG2 and MCF-7 cancer cell lines, with IC<sub>50</sub> values of 85.8 and 104.7 µg/mL, respectively, while showing lower cytotoxicity toward normal Vero cells with an IC<sub>50</sub> value of 262.5 µg/mL. In antioxidant assays, the TiO<sub>2</sub> nanoparticles demonstrated DPPH and ABTS radical scavenging activities with IC<sub>50</sub> values of 319 and 211 µg/mL, respectively. The nanoparticles also showed significant antibiofilm activity against *Escherichia coli* and *Klebsiella pneumoniae*, achieving maximum inhibition rates of 76.4% and 57.5%, respectively. Furthermore, the synthesized TiO<sub>2</sub> nanoparticles displayed antidiabetic potential through inhibition of α-amylase and α-glucosidase enzymes, with inhibition percentages reaching 63.9% and 79.1%, respectively. Overall, the study showed that green-synthesized TiO<sub>2</sub> nanoparticles had multifunctional biological activities and may serve as promising eco-friendly nanomaterials for biomedical and therapeutic applications.

DOI: 10.15376/biores.21.3.6608-6623

Keywords: TiO<sub>2</sub> NPs; Characterization; Anticancer; Antioxidant; Antibiofilm

Contact information: a: Chemistry Department, College of Science, King Faisal University, Al-ahsa, Saudi Arabia; b: Department of Biology, College of Science, Princess Nourah bint Abdulrahman University, P.O. Box 84428, Riyadh 11671, Saudi Arabia; c: Department of Medical Laboratory, College of Applied Medical Sciences, Prince Sattam Bin Abdulaziz University, 11942 Alkharj, Saudi Arabia; d: Department of Public Health, College of Applied Medical Sciences, Qassim University, P.O. Box 6666, 51452 Buraydah, Saudi Arabia; e: Botany and Microbiology Department, Faculty of Science, Al-Azhar University, Nasr City 11884, Cairo, Egypt; \*Corresponding authors: Mohamed.k.yousef@azhar.edu.eg; Halmutairi@kfu.edu.sa

## INTRODUCTION

Nanoparticles have emerged as essential components in nanotechnology because of their remarkable physicochemical characteristics and broad range of applications across optical, structural, electronic, and biomedical fields (Soliman *et al.* 2023, 2024a). Their nanoscale dimensions and unique structural features impart enhanced physical, chemical, electrical, and optical properties, enabling their use in sensors, catalytic systems, antibacterial agents, and antioxidant applications (Soliman *et al.* 2024b). In recent years,

semiconductor metal oxide nanoparticles—such as TiO<sub>2</sub>, CuO, ZnO, SnO<sub>2</sub>, ZnS, and CdS—have attracted considerable attention owing to their significant roles in environmental remediation and biomedical applications (Karthikeyan *et al.* 2020). Among these, titanium dioxide (TiO<sub>2</sub>) has gained prominence as a transition metal oxide semiconductor because of its advantageous properties, including chemical stability, low cost, non-toxicity, ease of preparation, and strong resistance to chemical corrosion. These attributes make TiO<sub>2</sub> highly suitable for applications in chemical sensors, solar energy devices, and environmental purification technologies (Suwarnkar *et al.* 2017). Furthermore, titania is widely recognized for its safety to humans and the environment, excellent biocompatibility, and high chemical durability (Nabi *et al.* 2022). Due to its low toxicity, biodegradability, and biocompatibility, TiO<sub>2</sub> has also been extensively explored in biomedical fields such as drug delivery, cancer therapy, and antimicrobial treatments (Ma *et al.* 2017).

The synthesis of nanomaterials using plant resources, commonly referred to as phytosynthesis or green synthesis, has gained increasing interest as a sustainable alternative to conventional methods. In this approach, plant extracts act as natural reducing, capping, and stabilizing agents, where the inherent biomolecules impart unique functional properties to the synthesized nanomaterials (Soliman *et al.* 2025a). Green synthesis represents an environmentally friendly and economically viable strategy for producing various nanomaterials, including metals, metal oxides, sulfides, nitrides, and carbides. In response to the growing need to reduce reliance on costly and environmentally hazardous synthetic routes, green technologies offer biologically safe, ecologically benign, and cost-effective solutions (Lithi *et al.* 2025).

Although microwave-assisted synthesis was first introduced in synthetic chemistry during the 1980s, it has since evolved into a powerful and environmentally benign technique for producing metal oxide nanoparticles with controlled sizes and morphologies (Krishnakumar *et al.* 2009). Microwave irradiation offers several advantages, including rapid reaction rates, uniform volumetric heating, enhanced selectivity, and improved product yields (Zhu *et al.* 2008). Previous reports have demonstrated that metal oxide nanoparticles synthesized *via* microwave irradiation exhibit enhanced photocatalytic and antimicrobial activities, as exemplified by ZnO nanoparticles produced using this method (Mallikarjunaswamy *et al.* 2020). In green TiO<sub>2</sub> synthesis, the plant extract mainly acts as a stabilizing and capping agent, while TiO<sub>2</sub> formation proceeds through hydrolysis and condensation rather than direct reduction of Ti<sup>4+</sup> ions, since titanium retains the same oxidation state in both the precursor and the final oxide product (Ansari *et al.* 2022)

Accordingly, the present study was undertaken to synthesize TiO<sub>2</sub> nanoparticles using lemon peel extract *via* a microwave-assisted green synthesis approach. The prepared sample were systematically characterized using TEM, DLS, FT-IR, UV-Visible spectroscopy, and SEM-EDX. Furthermore, the biomedical potential of the TiO<sub>2</sub> nanoparticles was evaluated through comprehensive *in vitro* assessments, including anticancer, antioxidant, antibiofilm, and antidiabetic activities.

## MATERIALS AND METHODS

### Preparation of Lemon Peel Extract

Lemon peels were collected from the Aman market, thoroughly washed with tap and double-distilled water, air-dried, and cut into small pieces. Fifty grams of the dried

peels were boiled in 200 mL of distilled water at 75 to 80 °C for 4 h. The mixture was cooled, filtered using Whatman No. 1 filter paper, and the resulting lemon peel extract (LPE) was stored at 4 °C for further use (Anigol *et al.* 2023).

### Microwave-Assisted Green Synthesis of TiO<sub>2</sub> NPs

TiO<sub>2</sub> NPs were synthesized by mixing 100 mL of lemon peel extract (LPE) with 900 mL of a 25 mM aqueous solution of titanium tetrachloride (TiCl<sub>4</sub>) under continuous stirring at 60 °C. After 2 h, the reaction mixture was subjected to microwave irradiation at 800 W and 2450 MHz for 10 min. The temperature during microwave irradiation was monitored and maintained at approximately 60 °C. The synthesis procedure was repeated under identical experimental conditions to ensure reproducibility of the results. The formed nanoparticles were collected by centrifugation at 12,000 rpm for 20 min, washed repeatedly with distilled water and ethanol (1:1, v/v), and dried at 95 °C for 12 h. Finally, the dried product was calcined at 550 °C for 6 h to obtain crystalline TiO<sub>2</sub> NPs, which were stored for further characterization and biological assays (Anigol *et al.* 2023; Al Masoudi *et al.* 2023).

### Characterization Studies of TiO<sub>2</sub> Nanoparticles

The formation of TiO<sub>2</sub> NPs was initially indicated by a visible color change in the reaction mixture during incubation. UV–Vis spectroscopy (Jenway 6305) was used to monitor nanoparticle synthesis over a wavelength range of 200 to 800 nm. Surface functional groups of the synthesized TiO<sub>2</sub> NPs were identified using FTIR spectroscopy (PerkinElmer Spectrum Two) within the range of 400 to 4000 cm<sup>-1</sup>. The morphology and particle size were analyzed by transmission electron microscopy (TEM, JEOL-2010), while surface structure and particle distribution were examined using scanning electron microscopy (SEM, Zeiss EVO-MA 10). The composition of elements and purity were determined by SEM-coupled energy-dispersive X-ray analysis (EDX, Bruker). In addition, dynamic light scattering (DLS) was employed to evaluate particle size distribution in aqueous suspension (Selim *et al.* 2025; Soliman and Salem 2025).

### Anticancer Activity

The anticancer potential of the synthesized nanoparticles was evaluated against hepatocellular carcinoma (HepG2) and breast cancer (MCF-7) cell lines, with normal Vero cells used as a control. Cells were seeded in 96-well plates at a density of  $1 \times 10^5$  cells/mL (100 µL per well) and incubated at 37 °C for 24 h to allow monolayer formation. The culture medium was then removed, and cells were gently washed twice to eliminate non-adherent cells. Nanoparticle samples, prepared as serial dilutions in RPMI medium supplemented with 2% serum (15.7 to 1000 µg/mL), were added to the wells (100 µL/well), while control wells received medium only. After incubation, morphological alterations indicative of cytotoxicity including cell rounding, detachment, granulation, and monolayer disruption were examined microscopically. Cell viability was quantitatively determined using the MTT assay, in which metabolically active cells reduced MTT (5 mg/mL in PBS) to formazan crystals. The crystals were solubilized with 200 µL of DMSO under shaking, and absorbance was measured at 560 nm using a microplate reader to calculate cell viability (Soliman *et al.* 2025b; Soliman and Salem 2025b).

## Biofilm Inhibition Assay

The microtiter plate (MTP) assay was employed to evaluate the antibiofilm activity of TiO<sub>2</sub> NPs against biofilm-forming bacterial strains, *Escherichia coli* and *Klebsiella pneumoniae*, with minor modifications from previously described methods (Almuhayawi *et al.* 2024; Soliman *et al.* 2024c). Briefly, TiO<sub>2</sub> NPs at different concentrations were added to flat-bottom 96-well microtiter plates containing tryptic soy broth (TSB) supplemented with 1% glucose. Overnight bacterial cultures were diluted at a ratio of 1:100 in TSB to achieve a final cell density of approximately  $1.5 \times 10^6$  CFU/mL. The prepared suspensions were aliquoted into the wells of microtiter plates and incubated at 37 °C for 48 h to promote biofilm development. After incubation, planktonic cells were carefully removed, and the wells were gently washed several times with PBS at pH 7.4 to eliminate non-adherent cells. The adhered biofilms were fixed with 200 µL of 95% methanol for 10 min, stained with 0.3% (w/v) crystal violet for 15 min at room temperature, and excess stain was removed by washing with sterile distilled water. For quantitative analysis, the bound crystal violet was solubilized using 30% acetic acid, and absorbance was measured at 540 nm using a microplate reader. Biofilm inhibition was calculated by comparing treated wells with untreated controls.

## Antioxidant Activity

### DPPH radical scavenging assay

The antioxidant activity of the synthesized nanoparticles was evaluated using the DPPH radical scavenging method. Different concentrations of the samples (15.7 to 1000 µg/mL) were prepared in methanol. Each concentration was mixed with a 1.0 mM methanolic solution of DPPH, while quercetin at corresponding concentrations served as a positive control. The reaction mixtures were incubated at 37 °C for 30 min in the dark, and the absorbance was measured at 515 nm using a UV–Vis spectrophotometer. A mixture of methanol and DPPH solution without sample was used as the blank. The percentage of DPPH radical scavenging activity was calculated using the following equation (Gulcin and Alwaseel 2023):

$$\text{DPPH scavenging (\%)} = \frac{A_{\text{control}} - A_{\text{sample}}}{A_{\text{control}}} \times 100 \quad (1)$$

### ABTS radical scavenging assay

The ABTS assay was performed using the ABTS<sup>•+</sup> radical cation generated by reacting 7 mM ABTS with 140 mM potassium persulfate, followed by incubation in the dark at room temperature for 12 to 16 h. The resulting solution was diluted with distilled water (1:3, v/v) to obtain an absorbance of approximately 0.7 at 734 nm. Sample solutions (15.7 to 1000 µg/mL) were mixed with the ABTS reagent in a 1:1 ratio and incubated at 37 °C for 6 min in the dark. Absorbance was then recorded at 734 nm using a UV–Vis spectrophotometer (Hanafy *et al.* 2021; Sahin *et al.* 2025). The percentage of ABTS radical scavenging activity and IC<sub>50</sub> values were calculated using the equation:

$$\text{Scavenging activity (\%)} = \frac{A_{\text{control}} - A_{\text{sample}}}{A_{\text{control}}} \times 100 \quad (2)$$

## Antidiabetic Activity

### α-Glucosidase inhibition assay

The α-glucosidase inhibitory activity of TiO<sub>2</sub> NPs was evaluated using yeast α-glucosidase with *p*-nitrophenyl-α-D-glucopyranoside (pNPG) as the substrate. Test samples and reference inhibitors were prepared in PBS (phosphate-buffered saline) at doses

ranging from 1.95 to 1000  $\mu\text{g/mL}$ . The enzyme solution (1 U/mL in 0.1 M PBS) was incubated with the test samples at 37 °C for 20 min. Subsequently, pNPG (10 mM) was added to initiate the reaction, followed by incubation at 37 °C for 30 min. The reaction was terminated by the addition of 1 M sodium carbonate, and absorbance was measured at 405 nm using a microplate reader. The percentage inhibition of  $\alpha$ -glucosidase activity was calculated based on absorbance values as previously described (Kim *et al.* 2004).

#### *$\alpha$ -Amylase inhibition assay*

The inhibitory effect of TiO<sub>2</sub> NPs on  $\alpha$ -amylase activity was determined using the dinitrosalicylic acid (DNSA) method. The TiO<sub>2</sub> NPs suspensions and standard inhibitors were prepared in PBS at concentrations of 1.95 to 1000  $\mu\text{g/mL}$ . The reaction mixture, consisting of  $\alpha$ -amylase (2 U/mL) and test samples, was incubated at 37 °C for 20 min. A 1% (w/v) potato starch solution prepared in PBS was then added as the substrate, followed by further incubation at 37 °C for 30 min. The enzymatic reaction was stopped by adding DNSA reagent, and the mixture was heated at 90 °C for 10 min. After cooling, the absorbance was recorded at 540 nm. The percentage inhibition of  $\alpha$ -amylase activity was calculated according to the method reported by Wickramaratne *et al.* (2016).

#### Statistical Analysis

All experimental data were processed using GraphPad Prism software (version 8.0; GraphPad Software Inc., San Diego, CA, USA). Comparisons among multiple groups were conducted using one-way or two-way analysis of variance (ANOVA), followed by Tukey's HSD post hoc test for pairwise multiple comparisons. Statistical significance was defined as a probability level of  $P < 0.05$ . All experiments were performed in triplicate ( $n = 3$ ), and the data are expressed as mean  $\pm$  standard deviation (SD).

## RESULTS AND DISCUSSION

### Characterization of TiO<sub>2</sub> Nanoparticles

The UV–Vis absorption spectrum of the biosynthesized TiO<sub>2</sub> NPs is presented in Fig. 1a. A distinct absorbance peak was observed at 297 nm within the wavelength range of 200 to 800 nm, confirming the successful formation of TiO<sub>2</sub> NPs using LPE. This absorbance band is characteristic of TiO<sub>2</sub> NPs and is consistent with previously reported green-synthesized TiO<sub>2</sub> systems (Maheswari *et al.* 2020). Comparable absorption features have been reported for TiO<sub>2</sub> NPs biosynthesized using *Juniperus phoenicea* leaf extract, which exhibited a characteristic peak at 205 nm (Al Masoudi *et al.* 2023). Figure 1b illustrates the FT-IR spectra of TiO<sub>2</sub> NPs obtained through microwave-assisted green synthesis, recorded over the range of 400 to 4000  $\text{cm}^{-1}$ . The spectra exhibit characteristic absorbance bands at 2916, 2849, 1732, 1615, 1417, 1003, 786, 541, and 444  $\text{cm}^{-1}$ , confirming the successful formation of TiO<sub>2</sub> NPs and the effective involvement of LPE as a capping and stabilizing agent.

The presence of multiple bands in the high-frequency region indicates surface functionalization of the nanoparticles by phytochemicals, a hallmark advantage of green synthesis routes that enhances nanoparticle stability (Darwich *et al.* 2025; (Aljohani *et al.* 2026). Specifically, the absorbance bands at 2916 and 2849  $\text{cm}^{-1}$  correspond to asymmetric and symmetric C–H stretching vibrations of methylene ( $-\text{CH}_2$ ) groups, commonly associated with fatty acids, lipids, or long-chain alcohols present in plant extracts (Kumar

*et al.* 2017). The prominent band at  $1732\text{ cm}^{-1}$  is attributed to C=O stretching vibrations of carbonyl groups, such as esters, aldehydes, or ketones derived from plant metabolites (Fowsiya *et al.* 2016). In addition, the bands observed at  $1615$  and  $1417\text{ cm}^{-1}$  are assigned to asymmetric and symmetric stretching vibrations of carboxylate ( $\text{COO}^-$ ) groups, respectively. The separation between these bands ( $\sim 198\text{ cm}^{-1}$ ) suggests bidentate or bridging coordination of carboxylate groups to surface titanium ions, indicating strong interaction between phytochemicals and the  $\text{TiO}_2$  NPs surface (Marstin *et al.* 2018). The band at  $1003\text{ cm}^{-1}$  is associated with C–O stretching vibrations of alcohols or polysaccharides, further supporting phytochemical capping (Rajan *et al.* 2015). The fingerprint region below  $800\text{ cm}^{-1}$  provides definitive evidence for  $\text{TiO}_2$  formation. The absorbance bands at  $786$ ,  $541$ , and  $444\text{ cm}^{-1}$  are characteristic of Ti–O–Ti stretching vibrations within the  $\text{TiO}_2$  lattice (Srujana *et al.* 2022). Notably, the peaks at  $541$  and  $444\text{ cm}^{-1}$  are indicative of the  $\text{TiO}_2$ , which is widely recognized for its superior photocatalytic and biomedical performance (Ahmad *et al.* 2022).

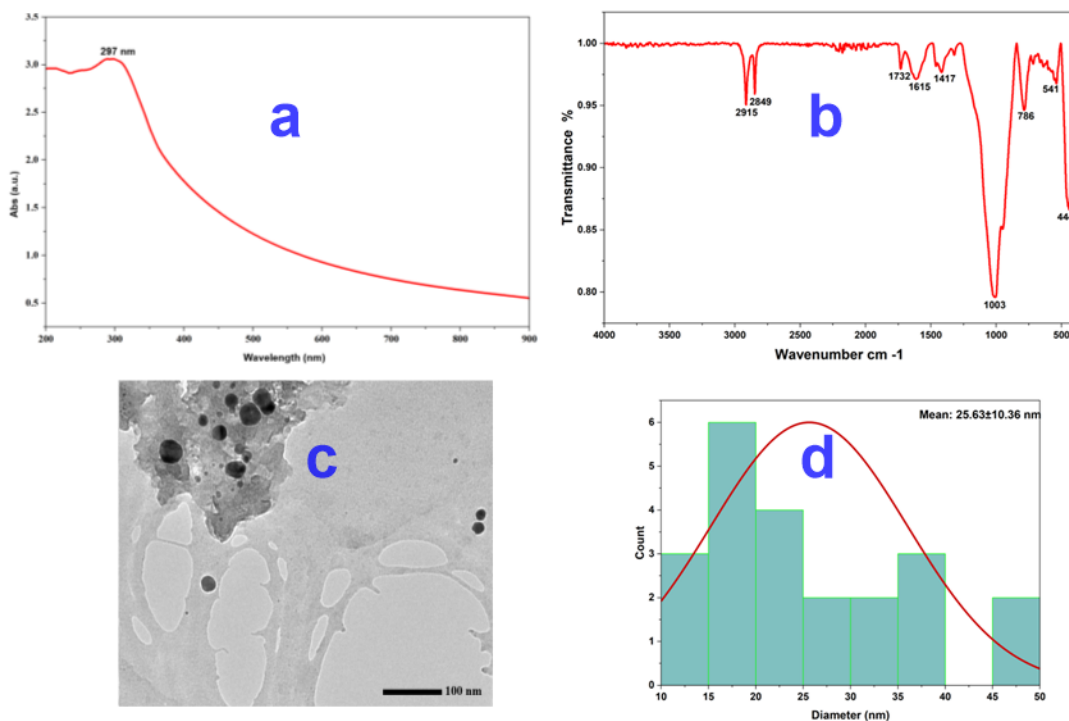


**Fig. 1.** Characterization of synthesized  $\text{TiO}_2$  NPs: (a) UV–Vis spectrum, (b) FTIR analysis, (c) TEM image, and (d) particle size distribution

Transmission electron microscopy (TEM) was employed to examine the morphology and size distribution of the synthesized nanoparticles. The TEM images (Fig. 1c) reveal predominantly spherical  $\text{TiO}_2$  NPs with a relatively uniform morphology. Particle size distribution analysis (Fig. 1d) showed an average particle size of approximately 25.6 nm.

The narrow size distribution and limited polydispersity suggest that microwave-assisted synthesis provided rapid and homogeneous energy transfer, promoting uniform nucleation and controlled particle growth (Jalaw Khan *et al.* 2020). This uniform heating is a key advantage of microwave irradiation, enabling the simultaneous formation of nanoparticles with consistent sizes throughout the reaction medium (Bilecka and Niederberger 2010).

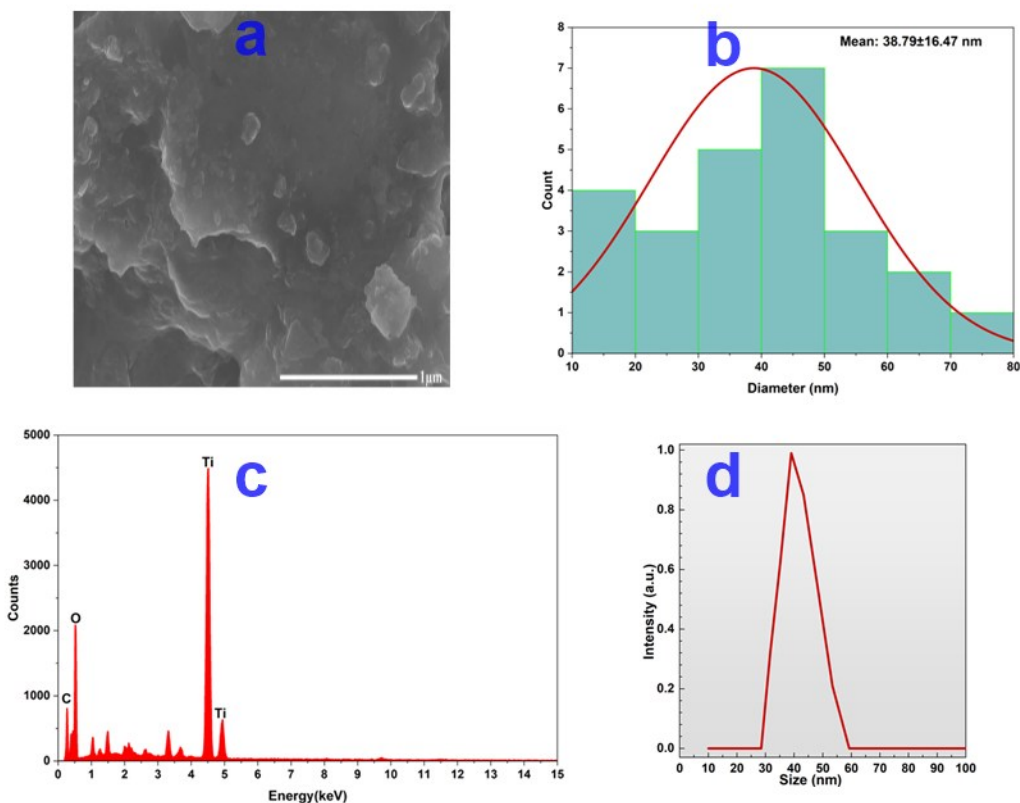


**Fig. 2.** (a) SEM image, (b) particle size distribution histogram, (c) EDX spectrum, and (d) DLS size distribution profile of the synthesized TiO<sub>2</sub> NPs

The SEM images revealed predominantly spherical nanoparticles with a relatively uniform distribution (Fig. 2a). The average particle size estimated from SEM analysis was approximately 38.7 nm (Fig. 2b). The slightly larger particle size observed in SEM compared to TEM can be attributed to the interaction volume of the electron beam and the presence of an organic capping layer on the nanoparticle surface, whereas TEM provides a direct visualization of the particle core (Goldstein *et al.* 2017). The relatively small particle size and limited aggregation indicates that LPE acted effectively as a capping and stabilizing agent, thereby reducing nanoparticle agglomeration during synthesis. Elemental composition analysis using EDX (Fig. 2c) confirmed the presence of titanium (Ti) and oxygen (O), validating the formation of TiO<sub>2</sub> NPs. In addition, a distinct carbon (C) signal was detected, supporting the FTIR results and providing direct evidence for the organic capping layer derived from LPE surrounding the TiO<sub>2</sub> core (Marslin *et al.* 2018). The EDX spectrum further provided the weight and atomic percentages of the constituent elements, indicating the purity and elemental composition of the synthesized TiO<sub>2</sub> NPs. Dynamic light scattering analysis was employed to evaluate the particle size distribution of the green-synthesized TiO<sub>2</sub> NPs. The DLS histogram (Fig. 2d) shows a relatively narrow size distribution and the average hydrodynamic diameter of approximately 39.0 nm. This result indicates good colloidal stability and supports the effectiveness of the green synthesis approach in producing uniformly dispersed nanoparticles. The observed hydrodynamic size, which includes the solvated layer and surface-bound phytochemicals, is consistent with the SEM-estimated particle size. Comparable findings have been reported in previous studies, where green-synthesized TiO<sub>2</sub> NPs exhibited mean diameters in the range of 50 to

60 nm, while chemically synthesized TiO<sub>2</sub> NPs showed larger sizes (60 to 70 nm), further confirming the advantage of green synthesis routes in controlling particle growth and aggregation (Ramya *et al.* 2024). The smaller particle size observed by TEM (25.6 nm) represents the actual core size of TiO<sub>2</sub> nanoparticles. In contrast, the relatively larger sizes obtained by SEM (38.7 nm) and DLS (~39 nm) can be attributed to surface capping by phytochemicals from lemon peel extract, possible slight aggregation, and the hydrodynamic diameter measured in suspension.

### Anticancer Activity

The cytotoxicity of the biosynthesized TiO<sub>2</sub> NPs was initially tested upon Vero cells to evaluate their biocompatibility. As shown in Fig. 3a, TiO<sub>2</sub> NPs exhibited little toxic effect toward normal cells, with a relatively high IC<sub>50</sub> value of 262.5 µg/mL over the tested concentration range (15.7 to 1000 µg/mL), indicating good biocompatibility. Subsequently, the anticancer efficacy of TiO<sub>2</sub> NPs was assessed against hepatocellular carcinoma (HepG2) and breast cancer (MCF-7) cell lines. The nanoparticles displayed significant, dose-dependent cytotoxic effects against both cancer cell types. The calculated IC<sub>50</sub> values were 85.8 µg/mL for HepG2 cells and 104.7 µg/mL for MCF-7 cells, demonstrating pronounced and favorable anticancer materials relative to their minimal toxicity toward normal Vero cells. The selective cytotoxicity observed for cancer cells is a key feature of promising nanotherapeutic agents. This enhanced sensitivity may be attributed to the higher metabolic rate and more negatively charged membrane potential of cancer cells, which facilitate increased nanoparticle uptake *via* endocytosis. Following internalization, TiO<sub>2</sub> NPs are known to induce cytotoxicity through the generation of reactive oxygen species (ROS), even under low-light or dark conditions, leading to oxidative stress, mitochondrial dysfunction, and subsequent apoptotic or necrotic cell death (Ramesh *et al.* 2023). Differences in IC<sub>50</sub> values between HepG2 and MCF-7 cells may reflect variations in cellular metabolism, genetic background, antioxidant defense mechanisms, and nanoparticle internalization efficiency (Ibrahim *et al.* 2024). To support the quantitative MTT assay findings, cellular morphology was examined using an inverted microscope. Excessive ROS production leads to mitochondrial membrane depolarization, cytochrome c release, and subsequent activation of caspase cascades, ultimately triggering apoptotic cell death (Khan *et al.* 2022).

### Anti Biofilm Capability of TiO<sub>2</sub> NPs

The antibiofilm activity of the biosynthesized TiO<sub>2</sub> NPs was evaluated against two clinically relevant biofilm-forming bacterial strains, *Escherichia coli* and *Klebsiella pneumoniae*. Bacterial biofilms consist of highly organized microbial communities embedded within an extracellular polymeric substance (EPS) matrix, which provides substantial protection against antibiotics and host immune defenses, making biofilm disruption a major therapeutic challenge (Vestby *et al.* 2020). The results demonstrated that TiO<sub>2</sub> NPs exerted a marked, concentration-dependent inhibitory effect on biofilm formation in both tested strains (Fig. 3b). In the case of *E. coli*, the nanoparticles showed strong antibiofilm efficacy, with inhibition reaching 76.4% at 1000 µg mL<sup>-1</sup> and decreasing to 20.9% at the lowest tested concentration (15.7 µg mL<sup>-1</sup>). Notably, this substantial reduction in biofilm biomass occurred without a pronounced effect on planktonic bacterial growth, indicating a targeted antibiofilm action rather than bactericidal activity. In contrast, TiO<sub>2</sub> NPs displayed comparatively lower antibiofilm efficiency against *K. pneumoniae*, achieving a maximum inhibition of 57.5% at 1000 µg mL<sup>-1</sup>. This reduced susceptibility is

consistent with the known biological characteristics of *K. pneumoniae*, which produces a thick polysaccharide capsule and forms highly resilient biofilms that are less permeable to antimicrobial agents and nanomaterials (Li *et al.* 2024). Variations in EPS composition, surface charge, and the regulation of biofilm-associated virulence factors between the two bacterial species likely contribute to the observed differences in nanoparticle effectiveness (Khatoon *et al.* 2018). Although the precise mechanism underlying TiO<sub>2</sub> NP-mediated biofilm inhibition remains to be fully elucidated, the observed activity may result from a combination of factors, including nanoparticle interaction with the EPS matrix, interference with cell–surface adhesion, disruption of biofilm architecture, and charge-mediated interactions that hinder biofilm maturation (Wang *et al.* 2017). Further studies employing microscopic and molecular approaches are warranted to clarify the direct effects of TiO<sub>2</sub> NPs on biofilm structure and integrity.

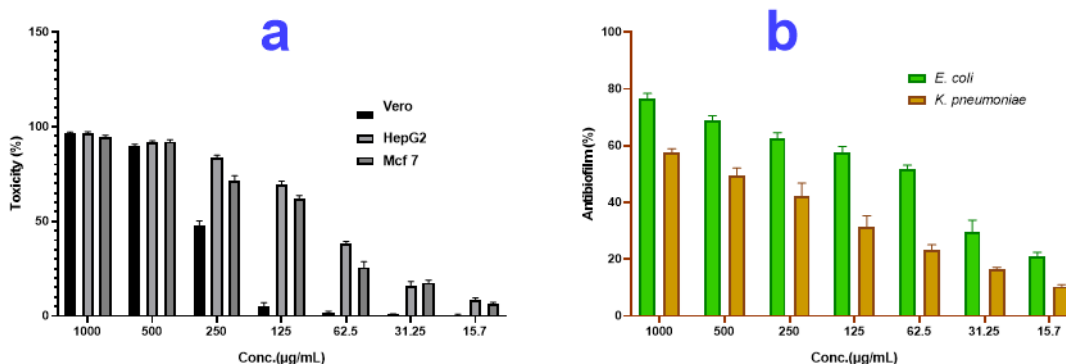


**Fig. 3.** (a) Cytotoxic activity against Vero, HepG2, and MCF-7 cell lines, and (b) Antibiofilm activity against *E. coli* and *K. pneumoniae* at different concentrations

### Antioxidant Activity

In the DPPH assay, the antioxidant activity was monitored through the discoloration of the purple DPPH solution, which reflects radical neutralization. The TiO<sub>2</sub> NPs exhibited a clear concentration-dependent scavenging effect over the tested range of 15.7 to 1000 µg/mL (Fig. 4a). The observed antioxidant activity may also be partially attributed to phytochemical residues from LBE adsorbed on the nanoparticle surface, which are known to possess radical scavenging properties. The calculated IC<sub>50</sub> value for DPPH radical inhibition was 319.4 µg mL<sup>-1</sup>, whereas the standard antioxidant ascorbic acid showed a significantly lower IC<sub>50</sub> of 59.2 µg mL<sup>-1</sup>, indicating stronger activity of the reference compound. The ABTS radical scavenging capacity of the TiO<sub>2</sub> NPs was also evaluated across the same concentration range. As presented in Fig. 4b, the nanoparticles demonstrated a pronounced dose-dependent ability to quench ABTS radicals. At the lowest tested concentration (15.7 µg mL<sup>-1</sup>), the scavenging efficiency was approximately 10.4%, which increased progressively to over 60.7% at 1000 µg mL<sup>-1</sup>. Based on the dose–response curves, the IC<sub>50</sub> value for ABTS scavenging by TiO<sub>2</sub> NPs was calculated to be 211 µg mL<sup>-1</sup>, compared with 104 µg mL<sup>-1</sup> for the reference antioxidant. Notably, the relatively stronger performance observed in the ABTS assay suggests that the biosynthesized TiO<sub>2</sub> NPs may act as efficient electron donors. This behavior can be attributed to surface defect states of TiO<sub>2</sub> as well as the synergistic contribution of phytochemical capping agents derived from the lemon peel extract, which enhance electron transfer and radical stabilization (Fu *et al.* 2024).

### Anti-diabetic Activity of TiO<sub>2</sub> NPs

The antidiabetic efficacy of the biosynthesized TiO<sub>2</sub> NPs was assessed by examining their inhibitory effects on the carbohydrate-hydrolyzing enzymes  $\alpha$ -amylase and  $\alpha$ -glucosidase, which play a central role in postprandial glucose regulation. Suppression of these enzymes is a well-established therapeutic approach for controlling hyperglycemia, as it slows the conversion of complex carbohydrates into absorbable monosaccharides, thereby moderating glucose uptake into the bloodstream (Debele and Park 2022). The results revealed that TiO<sub>2</sub> nanoparticles exerted a pronounced, dose-dependent inhibitory effect on both enzymes (Figs. 4c, 4d). At the highest tested concentration (1000  $\mu\text{g mL}^{-1}$ ), inhibition levels of 63.9% for  $\alpha$ -amylase and 79.1% for  $\alpha$ -glucosidase were achieved. In comparison, the standard antidiabetic drug acarbose exhibited stronger inhibition, reaching 95.6% and 95.8% against  $\alpha$ -amylase and  $\alpha$ -glucosidase, respectively, at the same concentration.

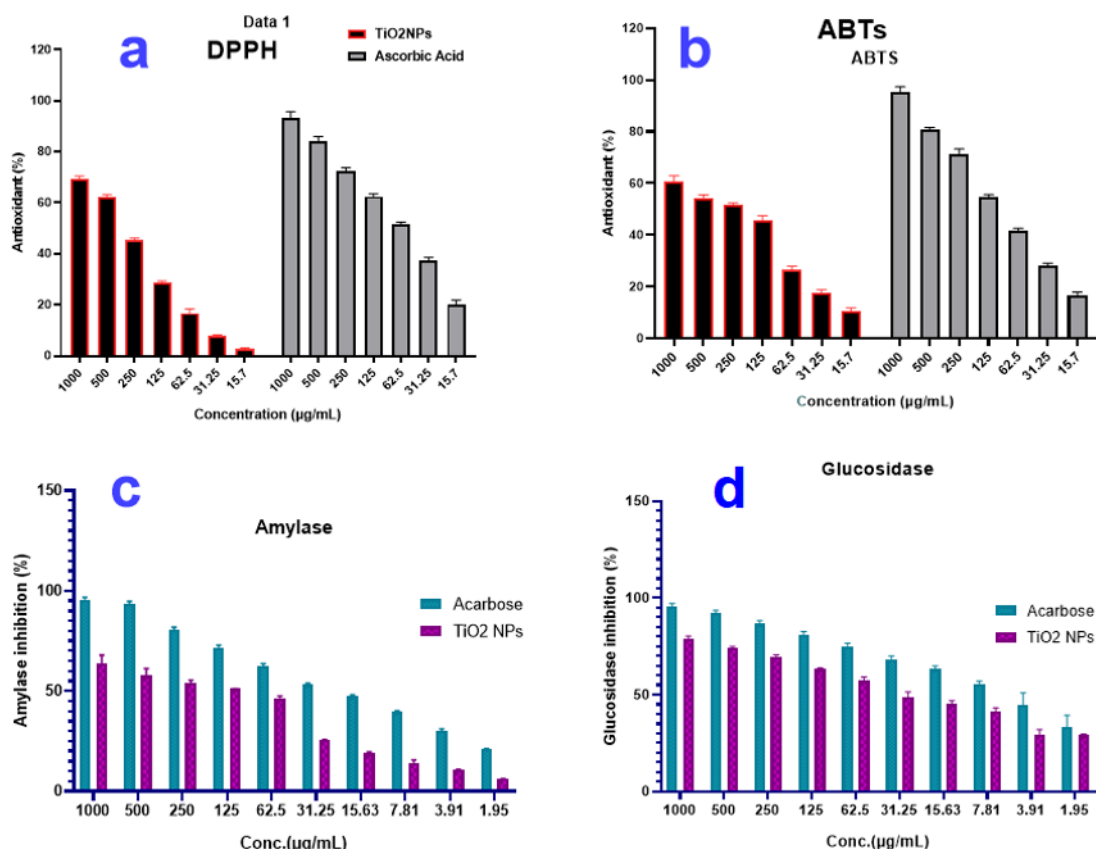


**Fig. 4.** (a) DPPH radical scavenging activity, (b) ABTS radical scavenging activity, (c)  $\alpha$ -amylase inhibitory activity, and (d)  $\alpha$ -glucosidase inhibitory activity compared with standard compounds of the synthesized TiO<sub>2</sub> nanoparticles

The observed enzyme inhibition by TiO<sub>2</sub> NPs may be attributed to a synergistic mechanism involving both the inorganic nanoparticle core and the phytochemical capping layer derived from the lemon peel extract. Bioactive compounds such as flavonoids and phenolic constituents are known to possess intrinsic inhibitory activity against digestive enzymes and may enhance the overall antidiabetic performance of the nanomaterial (Tundis *et al.* 2010). Additionally, the high surface-to-volume ratio and unique electronic properties of TiO<sub>2</sub> nanoparticles may promote strong interactions with enzyme surfaces,

leading to conformational alterations that reduce catalytic efficiency (Kumaravelu *et al.* 2025).

## CONCLUSIONS

1. TiO<sub>2</sub> nanoparticles (NPs) were successfully synthesized *via* an efficient microwave-assisted green method using lemon peel extract.
2. The nanoparticles showed spherical morphology with particle sizes ranging from 25 to 38 nm, which was confirmed by UV–Vis, Fourier transform infrared (FTIR), transmission electron microscope (TEM), and scanning electron microscope-energy-dispersive X-ray (SEM–EDX) analyses.
3. The TiO<sub>2</sub> NPs exhibited notable anticancer activity against HepG2 and MCF-7 cell lines.
4. The nanoparticles demonstrated antioxidant, antidiabetic, and antibiofilm activities, including effective inhibition of  $\alpha$ -amylase,  $\alpha$ -glucosidase, and biofilm formation in *K. pneumoniae* and *E. coli*.
5. Overall, the biosynthesized TiO<sub>2</sub> NPs show promising multifunctional biological activities under *in vitro* conditions. However, further *in vivo* and clinical studies are required to confirm their safety, efficacy, and potential for practical biomedical applications.
- 6.

## ACKNOWLEDGMENT

This work was funded by Princess Nourah bint Abdulrahman University Researchers Supporting Project number (PNURSP2026R62), Princess Nourah bint Abdulrahman University, Riyadh, Saudi Arabia. This work was supported by the Deanship of Scientific Research, Vice Presidency for Graduate Studies and Scientific Research, King Faisal University, Saudi Arabia (Grant No KFU262612).

## REFERENCES CITED

- Ahmad, M. Z., Alasiri, A. S., Ahmad, J., Alqahtani, A. A., Abdullah, M. M., Abdel-Wahab, B. A., Pathak, K., Saikia, R., Das, A., and Sarma, H. (2022). “Green synthesis of titanium dioxide nanoparticles using *Ocimum sanctum* leaf extract: *In vitro* characterization and its healing efficacy in diabetic wounds,” *Molecules* 27(22), article 7712. <https://doi.org/10.3390/molecules27227712>
- Aljohani, M. M., Khasim, S., Albalawi, M. E., Alfadhli, S., Ali, M. M., Waraky, A., Darwich, N. A., Khalil, M. I., and Hamdalla, T. A. (2026). “Green synthesis of silver and silver oxide nanoparticles from *Cedrus libani*: biological activity and influence of film thickness on optical properties,” *Ukrainian Journal of Physical Optics* 27, 1080-1101. <https://doi:10.3116/16091833/Ukr.J.Phys.Opt.2026.01080>
- Al Masoudi, L. M., A. Alqurashi, S., Abu Zaid, A., and Hamdi, H. (2023). “Characterization and biological studies of synthesized titanium dioxide nanoparticles

- from leaf extract of *Juniperus phoenicea* (L.) growing in Taif Region, Saudi Arabia,” *Processes* 11(1), article 272. <https://doi.org/10.3390/pr11010272>
- Almuhayawi, M. S., Alruhaili, M. H., Soliman, M. K., Tarabulsi, M. K., Ashy, R. A., Saddiq, A. A., Selim, S., Alruwaili, Y., and Salem, S. S. (2024). “Investigating the in vitro antibacterial, antibiofilm, antioxidant, anticancer and antiviral activities of zinc oxide nanoparticles biofabricated from *Cassia javanica*,” *Plos One* 19(10), article e0310927. <https://doi.org/10.1371/journal.pone.0310927>
- Anigol, L., Sajjan, V. and Gurubasavaraj, P. (2023). “Evaluation of antioxidant and antibacterial property of microwave assisted green synthesis of Fe<sub>3</sub>O<sub>4</sub>-MgO nanocomposites,” *IJST* 16(24), 1777-1786. <https://doi.org/10.17485/IJST/v16i24.629>
- Ansari, A., Siddiqui, V. U., Rehman, W. U., Akram, M. K., Ahmad, W., Siddiqi, A. M., Alosaimi, A. M., Hussein, M. A., and Rafatullah, M. (2022). “Green synthesis of TiO<sub>2</sub> nanoparticles using *Acorus calamus* leaf extract and evaluating its photocatalytic and in vitro antimicrobial activity,” *Catalysts* 12, article 181. <https://doi.org/10.3390/catal12020181>
- Bilecka, I., and Niederberger, M. (2010). “Microwave chemistry for inorganic nanomaterials synthesis,” *Nanoscale* 2(8), 1358-1374. <https://doi.org/10.1039/B9NR00377K>
- Darwich, N. A., Mezher, M., Abdallah, A. M., Hachem, Z., El-Sayed, A. F., El Hajj, R., Hamdalla, T. A., and Khalil, M. I. (2025). “Silver and yttrium-doped silver nanoparticles from pine needle leaf extract: synthesis, characterization, antioxidant, antiuropathogenic bacterial, and docking activities,” *Bioinorganic Chemistry and Applications* 2025, article 1566870. <https://doi.org/10.1155/bca/1566870>
- Debele, T. A., and Park, Y. (2022). “Application of nanoparticles: diagnosis, therapeutics, and delivery of insulin/anti-diabetic drugs to enhance the therapeutic efficacy of diabetes mellitus,” *Life* 12(12), article 2078. <https://doi.org/10.3390/life12122078>
- Fowsiya, J., Madhumitha, G., Al-Dhabi N. A., and Arasu, M. V. (2016). “Photocatalytic degradation of Congo red using *Carissa edulis* extract capped zinc oxide nanoparticles,” *Journal of Photochemistry and Photobiology B: Biology* 162, 395-401. <https://doi.org/10.1016/j.jphotobiol.2016.07.011>
- Fu, Q., Wei, C., and Wang, M. (2024). “Transition-metal-based nanozymes: synthesis, mechanisms of therapeutic action, and applications in cancer treatment,” *ACS Nano* 18(19), 12049-12095. <https://doi.org/10.1021/acsnano.4c02265>
- Goldstein, J., Newbury, D. E., Joy, D. C., Lyman, C. E., Echlin, P., Lifshin, E., Sawyer, L., and Michael, J. R. (2017). *Scanning Electron Microscopy and X-ray Microanalysis*, Springer, New York, USA. <https://doi.org/10.1007/978-1-4939-6676-9>
- Hanafy, S. M., Abd El-Shafea, Y. M., Saleh, W. D., and Fathy, H. M. (2021). “Chemical profiling, in vitro antimicrobial and antioxidant activities of pomegranate, orange and banana peel-extracts against pathogenic microorganisms,” *Journal of Genetic Engineering and Biotechnology* 19(1), article 80. <https://doi.org/10.1186/s43141-021-00151-0>
- Ibrahim, I. A. A., Alzahrani, A. R., Alanazi, I. M., Shahzad, N., Shahid, I., Falemban, A. H., Nur Azlina, M. F., and Arulselvan, P. (2024). “Synthesis and characterization of graphene oxide/polyethylene glycol/folic acid/brucine nanocomposites and their anticancer activity on HepG2 cells,” *International Journal of Nanomedicine* 2024, 1109-1124. <https://doi.org/10.2147/IJN.S445206>
- Jalaw Khan, R. S., Ouda, A. A., Abdul-lettif, A. M., and Alosfur, F. K. M. (2020). “Effect of solvents on the morphology of TiO<sub>2</sub> nanoparticles prepared by microwave

- method,” *IOP Conference Series: Materials Science and Engineering*, IOP Publishing. <https://doi.org/10.1088/1757-899X/928/7/072159>
- Karthikeyan, C., Arunachalam, P., Ramachandran, K., Al-Mayouf, A. M., and Karuppuchamy, B. S. (2020). “Recent advances in semiconductor metal oxides with enhanced methods for solar photocatalytic applications,” *Journal of Alloys and Compounds* 828, article 154281. <https://doi.org/10.1016/j.jallcom.2020.154281>
- Khan, M. I., Hossain, M. I., Hossain, M. K., Rubel, M., Hossain, K., Mahfuz, A., and Anik, M. I. (2022). “Recent progress in nanostructured smart drug delivery systems for cancer therapy: a review,” *ACS Applied Biomaterials* 5(3), 971-1012. <https://doi.org/10.1021/acsabm.2c00002>
- Khatoon, Z., McTiernan, C. D., Suuronen, E. J., Mah, T.-F., and Alarcon, E. I. (2018). “Bacterial biofilm formation on implantable devices and approaches to its treatment and prevention,” *Heliyon* 4(12), article e01067. <https://doi.org/10.1016/j.heliyon.2018.e01067>
- Kim, Y.-M., Wang, M.-H., and Rhee, H.-I. (2004). “A novel  $\alpha$ -glucosidase inhibitor from pine bark,” *Carbohydrate Research* 339(3), 715-717. <https://doi.org/10.1016/j.carres.2003.11.005>
- Krishnakumar, T., Jayaprakash, R., Pinna, N., Singh, V., Mehta, B., and Phani, A. (2009). “Microwave-assisted synthesis and characterization of flower shaped zinc oxide nanostructures,” *Materials Letters* 63(2), 242-245. <https://doi.org/10.1016/j.matlet.2008.10.008>
- Kumar, B., Smita, K., Cumbal, L., and Debut, A. (2017). “Green synthesis of silver nanoparticles using Andean blackberry fruit extract,” *Saudi Journal of Biological Sciences* 24(1), 45-50. <https://doi.org/10.1016/j.sjbs.2015.09.006>
- Kumaravelu, P., Shanmugam, R., and Jayakodi, S. (2025). “Advancements in medicinal plant-derived trace element nanoparticles for diabetes mellitus therapy,” *BioNanoScience* 15(3), article 429. <https://doi.org/10.1007/s12668-025-02037-8>
- Li, L., Gao, X., Li, M., Liu, Y., Ma, J., Wang, X., Yu, Z., Cheng, W., Zhang, W., and Sun, H. (2024). “Relationship between biofilm formation and antibiotic resistance of *Klebsiella pneumoniae* and updates on antibiofilm therapeutic strategies,” *Frontiers in Cellular and Infection Microbiology* 14, article 1324895. <https://doi.org/10.3389/fcimb.2024.1324895>
- Lithi, I. J., Nakib, K. I. A., Chowdhury, A. S., and Hossain, M. S. (2025). “A review on the green synthesis of metal (Ag, Cu, and Au) and metal oxide (ZnO, MgO, Co<sub>3</sub>O<sub>4</sub>, and TiO<sub>2</sub>) nanoparticles using plant extracts for developing antimicrobial properties,” *Nanoscale Advances*. <https://doi.org/10.1039/d5na00037h>
- Ma, Y., Guo, Y., Wu, S., Lv, Z., Zhang, Q., and Ke, Y. (2017). “Titanium dioxide nanoparticles induce size-dependent cytotoxicity and genomic DNA hypomethylation in human respiratory cells,” *RSC Advances* 7(38), 23560-23572. <https://doi.org/10.1039/C6RA28272E>
- Maheswari, P., Harish, S., Navaneethan, M., Muthamizhchelvan, C., Ponnusamy, S., and Hayakawa, Y. (2020). “Bio-modified TiO<sub>2</sub> nanoparticles with *Withania somnifera*, *Eclipta prostrata* and *Glycyrrhiza glabra* for anticancer and antibacterial applications,” *Materials Science and Engineering: C* 108, article 110457. <https://doi.org/10.1016/j.msec.2019.110457>
- Mallikarjunaswamy, C., Ranganatha, V. L., Ramu, R., Nagaraju, and G. (2020). “Facile microwave-assisted green synthesis of ZnO nanoparticles: Application to photodegradation, antibacterial and antioxidant,” *Journal of Materials Science:*

- Materials in Electronics* 31(2), 1004-1021. <https://doi.org/10.1007/s10854-019-02612-2>
- Marslin, G., Siram, K., Maqbool, Q., Selvakesavan, R. K., Kruszka, D., Kachlicki, P., and Franklin, G. (2018). "Secondary metabolites in the green synthesis of metallic nanoparticles," *Materials* 11(6), article 940. <https://doi.org/10.3390/ma11060940>
- Nabi, G., Ain, Q.-U.-., Tahir, M. B., Nadeem Riaz, K., Iqbal, T., Rafique, M., Hussain, S., Raza, W., Aslam, I., and Rizwan, M. (2022). "Green synthesis of TiO<sub>2</sub> nanoparticles using lemon peel extract: Their optical and photocatalytic properties," *International Journal of Environmental Analytical Chemistry* 102(2), 434-442. <https://doi.org/10.1080/03067319.2020.1722816>
- Rajan, R., Chandran, K., Harper, S. L., Yun, S.-I., and Kalaichelvan, P. T. (2015). "Plant extract synthesized silver nanoparticles: An ongoing source of novel biocompatible materials," *Industrial Crops and Products* 70, 356-373. <https://doi.org/10.1016/j.indcrop.2015.03.015>
- Ramesh, S., Govarthanan, K., and Palaniappan, A. (2023). "TiO<sub>2</sub> nanostructures—a double edged sword: Current progress on their role in stem cells' differentiation, cancer therapy, and their toxicity issues," *Nanotoxicology* 17(2), 176-201. <https://doi.org/10.1080/17435390.2023.2199858>
- Ramya, R., Muthulakshmi, G., Sudhahar, S., and Bhaskaran, A. (2024). "Green synthesis and characterization studies of TiO<sub>2</sub> nanoparticles and its potential biological performance," *Nano-Structures and Nano-Objects* 39, article 101322. <https://doi.org/10.1016/j.nanoso.2024.101322>
- Sahin, Z., Sonmez, F., Avci, D., Duran, T., and Darwich, N. A. (2025). "Bioactive potential of *Cydonia oblonga* and *Diospyros kaki* vinegars: Phenolic content, antioxidant and GST inhibitory activity, and molecular docking studies," *BioMed Research International* 2025, article 6699595. <https://doi.org/10.1155/bmri/6699595>
- Selim, S., Soliman, M. K., M. Almuhayawi, S., Alruhaili, M. H., Gattan, H. S., Saddiq, A. A., Hagagy, N., Alzahrani, A. J., Al Jaouni, S. K., and Salem, S. S. (2025). "Green synthesis, characterization, molecular simulation, and in vitro biomedical application of magnesium oxide nanoparticles," *PLOS One* 20(9), article e0332367. <https://doi.org/10.1371/journal.pone.0332367>
- Soliman, M. K., Abu-Elghait, M., Salem, S. S., and Azab, M. S. (2024a). "Multifunctional properties of silver and gold nanoparticles synthesis by *Fusarium pseudonygamai*," *Biomass Conversion and Biorefinery* 14(22), 28253-28270. <https://doi.org/10.1007/s13399-022-03507-9>
- Soliman, M. K., Hashem, A. H., Al-Askar, A. A., AbdElgayed, G., and Salem, S. S. (2024b). "Green synthesis of silver nanoparticles from *Bauhinia variegata* and their biological applications," *Green Processing and Synthesis* 13(1), article 20240099. <https://doi.org/10.1515/gps-2024-0099>
- Soliman, M. K., and Salem, S. S. (2025a). "Comparative evaluation of antimicrobial, antibiofilm, antioxidant, antiviral, and antidiabetic activities of copper oxide nanoparticles biofabricated via *Opuntia ficus indica*," *Scientific Reports* 15(1), article 24823. <https://doi.org/10.1038/s41598-025-08878-3>
- Soliman, M. K., and Salem, S. S. (2025b). "Uncovering the potential of biofabricated *Ananas comosus* peel selenium nanoparticles for antibacterial, antibiofilm, suppression of virulence genes (can and LuxS), anticancer, and antioxidant properties," *BMC Biotechnology* 25(1), 1-21. <https://doi.org/10.1186/s12896-025-00999-x>

- Soliman, M. K., Salem, S. S., Abu-Elghait, M., and Azab, M. S. (2023). "Biosynthesis of silver and gold nanoparticles and their efficacy towards antibacterial, antibiofilm, cytotoxicity, and antioxidant activities," *Applied Biochemistry and Biotechnology* 195(2), 1158-1183. <https://doi.org/10.1007/s12010-022-04199-7>
- Soliman, M. K., Talib, A. H., Mahmoud, R., Ali, Z. A., Al-Haideri, H. H., Abalkhail, A., Binshaya, A. S., Salem, M. H., Al-Otibi, F. O., and Yassin, M. T. (2025a). "Ecofriendly magnesium oxide nanoparticles: Anticancer, antimicrobial, and antidiabetic potentials in vitro," *AMB Express* 15(1), 1-20. <https://doi.org/10.1186/s13568-025-01950-1>
- Soliman, M. K. Y., Doghish, A. S., Hashem, A. H., Abdel-Maksoud, M., El-Dakrouy, W. A., Alamri, A., Ebaid, H., Hasanin, M. S., and Saied, E. (2025b). "Novel trimetallic (TiO<sub>2</sub>-MgO-Au) nanoparticles: Biosynthesis, characterization, antimicrobial, and anticancer activities," *Green Processing and Synthesis* 14(1), article 20250007. <https://doi.org/10.1515/gps-2025-0007>
- Srujana, S., Anjamma, M., Alimuddin, B. S., Dhakar, R. C., Natarajan, S., and Hechhu, R. (2022). "A comprehensive study on the synthesis and characterization of TiO<sub>2</sub> nanoparticles using *Aloe vera* plant extract and their photocatalytic activity against MB dye," *Adsorption Science and Technology* 2022, article 7244006. <https://doi.org/10.1155/2022/7244006>
- Suwarnkar, M., Khadem, G., Babarm, S. M., and Garadkarm, K. (2017). "Microwave synthesis of In-doped TiO<sub>2</sub> nanoparticles for photocatalytic application," *Journal of Materials Science: Materials in Electronics* 28(22), 17140-17147. <https://doi.org/10.1007/s10854-017-7641-8>
- Tundis, R., Loizzo, M. R., and Menichini, F. (2010). "Natural products as  $\alpha$ -amylase and  $\alpha$ -glucosidase inhibitors and their hypoglycaemic potential in the treatment of diabetes: an update," *Mini Reviews in Medicinal Chemistry* 10(4), 315-331. <https://doi.org/10.2174/138955710791331007>
- Vestby, L. K., Grønseth, T., Simm, R., and Nesse, L. L. (2020). "Bacterial biofilm and its role in the pathogenesis of disease," *Antibiotics* 9(2), article 59. <https://doi.org/10.3390/antibiotics9020059>
- Wang, L., Hu, C., and Shao, L. (2017). "The antimicrobial activity of nanoparticles: present situation and prospects for the future," *International Journal of Nanomedicine*, 1227-1249. <https://doi.org/10.2147/IJN.S121956>
- Wickramaratne, M. N., Punchihewa, J., and Wickramaratne, D. (2016). "In-vitro alpha amylase inhibitory activity of the leaf extracts of *Adenanthera pavonina*," *BMC Complementary and Alternative Medicine* 16(1), article 466. <https://doi.org/10.1186/s12906-016-1452-y>

Zhu, P., Zhang, J., Wu, Z., and Zhang, Z. (2008). "Microwave-assisted synthesis of various ZnO hierarchical nanostructures: effects of heating parameters of microwave oven," *Crystal Growth and Design* 8(9), 3148-3153.  
<https://doi.org/10.1016/j.jece.2019.103370>

Article submitted: January 22, 2026; Peer review completed: May 2, 2026; Revised version received: May 6, 2026; Accepted: May 12, 2026; Published: June 3, 2026.  
DOI: 10.15376/biores.21.3.6608-6623